International Journal of Fracture **86:** 343–360, 1997.

Plane strain asymptotic fields for cracks terminating at the interface between elastic and pressure-sensitive dilatant materials

HONGRONG YU, YONG-LI WU[1] and GUOCHEN LI
Institute of Mechanics, Chinese Academy of Sciences, Beijing 100080, P. R. China
[1]*To whom all correspondence should be addressed.*

Received 20 August 1996; accepted in revised form 11 July 1997

Abstract. The plane strain asymptotic fields for cracks terminating at the interface between elastic and pressure-sensitive dilatant material are investigated in this paper. Applying the stress-strain relation for the pressure-sensitive dilatant material, we have obtained an exact asymptotic solution for the plane strain tip fields for two types of cracks, one of which lies in the pressure-sensitive dilatant material and the other in the elastic material and their tips touch both the bimaterial interface. In cases, numerical results show that the singularity and the angular variations of the fields obtained depend on the material hardening exponent n, the pressure sensitivity parameter μ and geometrical parameter λ.

Key words: Asymptotic field, interface crack, pressure-sensitive dilatant material

1. Introduction

Recently, research on the mechanical properties of some materials that exhibit pressure-sensitive dilatancy has attracted much attention because these materials cannot be described by the classical plasticity theories that assume that the hydrostatic pressure has little effect on material plastic deformation and neglects plastic dilatancy. Examples of these materials include toughened structural polymers and ceramics. According to studies by Spitzig and Richmond (1979), Carapellucci and Yee (1986), Sue and Yee (1989) and Chen and More (1986), it seems that pressure-sensitive yielding has a great effect on the plastic deformation and fracture of the materials studied.

Because defects emerge very easily in the interfacial regions, with the result that they are demolished, the interfaces play an important role for many engineering materials and much work on their crack-tip field has been published. Williams (1959), Cherpanov (1962), Erdogan (1965), Rice and Shih (1963, 1965) and Malyshev and Salganik (1965) analysed the elastic problem of a crack lying along the interface between two dissimilar isotropic media by utilizing different method. Recently Hutchinson et al. (1987), Rice (1988), Shih and Asaro (1988) and Zywicz and Park (1989) have summarized and developed these early research results. The solutions for an interface crack in elastic-plastic materials were investigated by Shih and Asaro (1988; 1990; 1989), Zywicz and Park (1989), Wang (1990). Yuan (1994/1995) has studied the problem of a plane strain crack lying along an interface between a rigid substrate and an elasto-plastic dilatant medium. Cook and Erdogan (1972) considered the problem of two elastic boned half-planes containing a crack perpendicular to the interface. Wang (1990) presented an exact asymptotic analysis for a crack lying in an elastic-plastic material and perpendicular to the interface of an elastic-plastic material and a linear elastic material. However, less attention has been paid to the crack terminating at a straight-line interface as

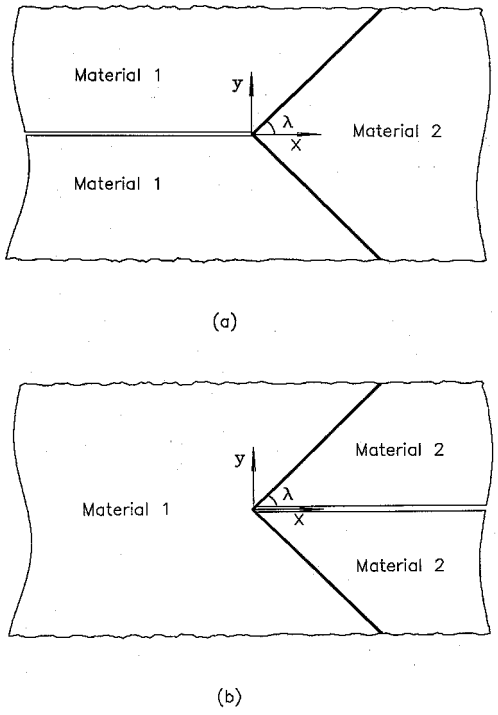

Figure 1. Geometry of a crack for bimaterial interface.

depicted in Figure 1, which may be the case during boundary fracturing of the composite or polycrystalline materials.

This paper investigates the plane strain asymptotic stress field near the crack tip between the pressure-sensitive dilatant material and the linear elastic material. Based on the pressure-sensitive yielding criterion introduced by Drucker and Prager (1952) and modified by Li and Pan (1990), an asymptotic solution for the stress-strain field near the crack tip is obtained for two types of cracks, one of which lies in pressure-sensitive dilatant material and its tip touches the bimaterial interface and the other in elastic material and its tip also touches the interface. The material constants n and μ and geometrical parameter λ are varied to examine their effects on the resulting stress and displacements distributions near the crack tip.

2. Constitutive relations

Consider a crack shown in Figure 1(a) which terminates at the interface between a linear elastic material with the region $-\lambda \leqslant \theta \leqslant \lambda$ (medium 2) and a pressure-sensitive dilatant material with the regions $\lambda \leqslant \theta \leqslant \pi$ and $-\pi \leqslant \theta \leqslant \lambda$ (medium 1). The external load is assumed to be the symmetrical remote tension. Due to symmetry we search only the solution in the region $0 \leqslant \theta \leqslant \pi$.

For the sake of simplicity, it is assumed that both materials have the same elastic modulus and Poisson's ratio, i.e. $E_1 = E_2 = E$, $\nu_1 = \nu_2 = \nu$.

For the plane strain, the stress-strain relation for material 2 can be expressed as

$$\varepsilon_{ij} = \frac{1+\nu}{E} S_{ij} + \frac{1-2\nu}{3E} \sigma_{kk} \delta_{ij}. \tag{1}$$

According to Li and Pan (1990) the following simple pressure-sensitive yielding criterion for material 1 is adopted

$$\tau_{ge} = \tau_e + \mu \sigma_m = \psi(\sigma_{ij}), \tag{2a}$$

$$\tau_e = (S_{ij} S_{ij}/2)^{1/2}, \quad S_{ij} = \sigma_{ij} - \sigma_m \delta_{ij}, \quad \sigma_m = \sigma_{kk}/3, \tag{2b}$$

where $\psi(\sigma_{ij})$ represents the yield surface in stress space, τ_{ge} is the generalized effective shear stress and μ is a pressure-sensitive factor. When $\mu = 0$, it means that the effect of hydrostatic pressure is neglected.

In this analysis, it is assumed that the elastic-plastic behaviour for material 1 in shear can be expressed as

$$\frac{\gamma}{\gamma_0} = \frac{\tau}{\tau_0} + \alpha \left(\frac{\tau}{\tau_0} \right)^n, \tag{3}$$

where τ and γ are respectively the shear stress and shear strain, τ_0 and γ_0 are the reference shear stress and reference strain, n is the strain hardening exponent and α is a material constant.

In an asymptotic analysis for a near-crack-tip field, the elastic strains are much smaller in comparison with the plastic stains and, therefore, can be neglected. In this sense, we have the constitutive equation

$$\frac{\varepsilon_{ij}^p}{\gamma_0} = \alpha \left(\frac{\tau_{ge}}{\gamma_0} \right)^n \left(\frac{S_{ij}}{2\tau_e} + \frac{\mu}{3} \delta_{ij} \right). \tag{4}$$

For the plane strain we have

$$\varepsilon_{zz} = 0. \tag{5}$$

Introducing (5) in (4), the strain-stress relations can be written as

$$\frac{\varepsilon_{rr}}{\gamma_0} = \tfrac{1}{2} \alpha \left(\frac{\tau_{ge}}{\tau_0} \right)^n \left(\frac{\sigma_{rr} - \sigma_{\theta\theta}}{2\tau_e} + \mu \right), \tag{6a}$$

$$\frac{\varepsilon_{\theta\theta}}{\gamma_0} = \tfrac{1}{2} \alpha \left(\frac{\tau_{ge}}{\tau_0} \right)^n \left(\frac{\sigma_{\theta\theta} - \sigma_{rr}}{2\tau_e} + \mu \right), \tag{6b}$$

$$\frac{\varepsilon_{r\theta}}{\gamma_0} = \tfrac{1}{2} \alpha \left(\frac{\tau_{ge}}{\tau_0} \right)^n \frac{\sigma_{r\theta}}{\tau_e}, \tag{6c}$$

where

$$\tau_e = \frac{\sigma_e}{\sqrt{3}} = (1 - \tfrac{1}{3}\mu^2)^{-1/2} \left[\left(\frac{\sigma_{rr} - \sigma_{\theta\theta}}{2} \right)^2 + \sigma_{r\theta}^2 \right]^{1/2},$$

$$\tau_{ge} = \frac{\sigma_{ge}}{\sqrt{3}} = (1 - \tfrac{1}{3}\mu^2)^{1/2} \left[\left(\frac{\sigma_{rr} - \sigma_{\theta\theta}}{2} \right)^2 + \sigma_{r\theta}^2 \right]^{1/2} + \frac{\mu}{2}(\sigma_{rr} + \sigma_{\theta\theta}).$$

The stress components in polar coordinates are expressed by the stress function $\phi(r, \theta)$ as

$$\sigma_{rr} = \frac{1}{r}\frac{\partial \varphi}{\partial r} + \frac{1}{r^2}\frac{\partial^2 \varphi}{\partial \theta^2}, \qquad \sigma_{\theta\theta} = \frac{\partial^2 \varphi}{\partial r^2}, \qquad \sigma_{r\theta} = -\frac{\partial}{\partial r}\left(\frac{1}{r}\frac{\partial \varphi}{\partial \theta} \right). \tag{7}$$

Then, the equations of equilibrium can be automatically satisfied.

The relations of the displacement strain are

$$\varepsilon_{rr} = \frac{\partial u_r}{\partial r}, \qquad \varepsilon_{\theta\theta} = \frac{1}{r}\frac{\partial u_\theta}{\partial \theta} + \frac{u_r}{r}, \qquad \varepsilon_{r\theta} = \frac{1}{2}\left(\frac{1}{r}\frac{\partial u_r}{\partial \theta} + \frac{\partial u_\theta}{\partial r} - \frac{u_\theta}{r} \right). \tag{8}$$

The strain compatibility equation is

$$\frac{1}{r}\frac{\partial^2 (r\varepsilon_{\theta\theta})}{\partial r^2} + \frac{1}{r^2}\frac{\partial^2 \varepsilon_{rr}}{\partial \theta^2} - \frac{1}{r}\frac{\partial \varepsilon_{rr}}{\partial r} - \frac{2}{r^2}\frac{\partial^2 (r\varepsilon_{r\theta})}{\partial r \partial \theta} = 0. \tag{9}$$

In order to ensure the tractions are to be continuous on the interface, we assume that the stress field in the whole tip zone has the same singularity for both materials. Let

$$\varphi(r, \theta) = K r^{s+2} F(\theta). \tag{10}$$

Substituting (10) into (7), we obtain

$$\sigma_{ij} = K r^s \tilde{\sigma}_{ij}(\theta), \tag{11}$$

$$\widetilde{\sigma}_{rr}(\theta) = F'' + (2 + s)F, \tag{12a}$$

$$\widetilde{\sigma}_{\theta\theta}(\theta) = (2 + s)(1 + s)F, \tag{12b}$$

$$\widetilde{\sigma}_{r\theta} = -(1 + s)F'. \tag{12c}$$

The corresponding stains can be written as

$$\varepsilon_{ij} = \widetilde{\alpha}\widetilde{K}^n r^{ns} \widetilde{\varepsilon}_{ij}, \tag{13}$$

$$\widetilde{\varepsilon}_{rr} = \tfrac{1}{2}\widetilde{\tau}_{ge}^n \left(\frac{\widetilde{\sigma}_{rr} - \widetilde{\sigma}_{\theta\theta}}{2\widetilde{\tau}_e} + \mu \right), \tag{14a}$$

$$\widetilde{\varepsilon}_{\theta\theta} = \tfrac{1}{2}\widetilde{\tau}_{ge}^n \left(\frac{\widetilde{\sigma}_{\theta\theta} - \widetilde{\sigma}_{rr}}{2\widetilde{\tau}_e} + \mu \right), \tag{14b}$$

$$\widetilde{\varepsilon}_{r\theta} = \tfrac{1}{2}\widetilde{\tau}_{ge}^n \frac{\widetilde{\sigma}_{r\theta}}{\widetilde{\tau}_e}, \tag{14c}$$

where

$$\widetilde{\tau}_e = \frac{\widetilde{\sigma}_e}{\sqrt{3}} = (1 - \tfrac{1}{3}\mu^2)^{-1/2} \left[\left(\frac{\widetilde{\sigma}_{rr} - \widetilde{\sigma}_{\theta\theta}}{2} \right)^2 + \widetilde{\sigma}_{r\theta}^2 \right]^{1/2},$$

$$\widetilde{\tau}_{ge} = \frac{\widetilde{\sigma}_{ge}}{\sqrt{3}} = (1 - \tfrac{1}{3}\mu^2)^{1/2} \left[\left(\frac{\widetilde{\sigma}_{rr} - \widetilde{\sigma}_{\theta\theta}}{2} \right)^2 + \widetilde{\sigma}_{r\theta}^2 \right]^{1/2} + \frac{\mu}{2}(\widetilde{\sigma}_{rr} + \widetilde{\sigma}_{\theta\theta}).$$

The strain compatibility (9) can be represented as

$$\left[\frac{\mathrm{d}^2}{\mathrm{d}\theta^2} - ns(ns-2) \right] \left[\widetilde{\tau}_{ge} \left(\frac{F'' - s(2+s)F}{\widetilde{\tau}_e} + 2\mu \right) \right]$$

$$+4(ns+1)(s+1)\frac{\mathrm{d}}{\mathrm{d}\theta}\left[\widetilde{\tau}_{ge}^n \frac{F'}{\widetilde{\tau}_e} \right] + 4\mu ns(ns+1)\widetilde{\tau}_{ge}^n = 0. \tag{15}$$

For the linear elastic material 2, we have the equation

$$F'''' + [(s+2)^2 + s^2]F'' + s^2(s+2)^2 = 0. \tag{16}$$

The general solution to Equation (16) for the symmetric remote tension is

$$F = B_1 \cos(s\theta) + B_3 \cos(s+2)\theta. \tag{17}$$

The traction-free conditions on the crack faces require

$$\sigma_{\theta\theta}|_{\theta=\pi} = \sigma_{r\theta}|_{\theta=\pi} = 0, \tag{18}$$

which means

$$F(\pi) = F'(\pi) = 0. \tag{19}$$

The continuity on the interface needs to have

$$\widetilde{\sigma}_{\theta\theta}(\lambda^+) = \widetilde{\sigma}_{\theta\theta}(\lambda^-), \quad \widetilde{\sigma}_{r\theta}(\lambda^+) = \widetilde{\sigma}_{r\theta}(\lambda^-). \tag{20}$$

From Equation (20) we get

$$F(\lambda^+) = F(\lambda^-), F'(\lambda^+) = F'(\lambda^-). \tag{21}$$

Ignoring the rigid displacements, we get from (8) the displacements for material 1

$$u_\beta = \alpha_l \widetilde{K} r^{(1+ns)} \widetilde{u}_\beta(\theta) \tag{22}$$

$$\widetilde{u}_r = \widetilde{\varepsilon}_l/(1+ns), \quad \widetilde{u}_\theta = (2\widetilde{\varepsilon}_{r\theta} - \widetilde{u}_r')/ns. \tag{23}$$

As pointed out by Shih and Asaro (1988) for the bimaterials, the material with a lower hardening capacity responds at the interface as if it is bonded to a rigid substance, so we have

$$\widetilde{u}_r = \widetilde{u}_\theta = 0, \quad \text{at } \theta = \lambda^+, \tag{24}$$

which can be written in terms of stresses as

$$\begin{aligned} &\widetilde{\sigma}_{rr} - \widetilde{\sigma}_{\theta\theta} + 2\mu\widetilde{\tau}_e = 0 \\ &\widetilde{\sigma}_{rr}' - \widetilde{\sigma}_{\theta\theta}' + 2\mu\widetilde{\tau}_e' - 4(ns+1)\widetilde{\sigma}_{r\theta} = 0 \end{aligned} \qquad \text{at } \theta = \lambda^+. \tag{25}$$

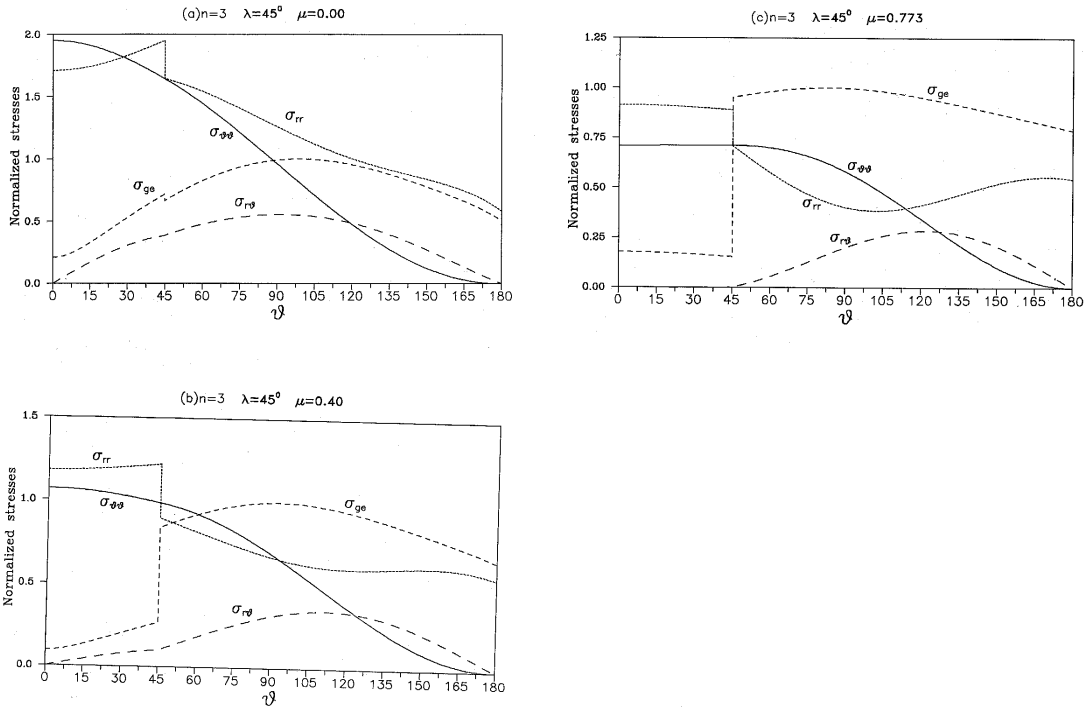

Figure 2. θ – variation of the normalized stresses for Figure 1(a) $(n = 3, \lambda = 45^{\circ})$.

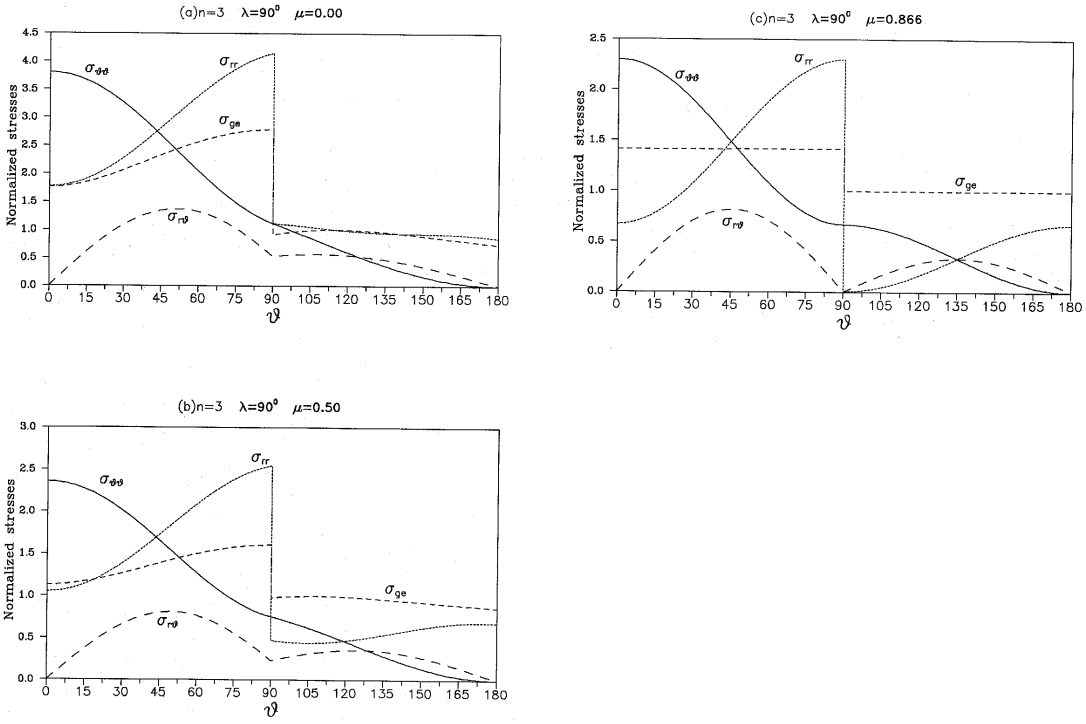

Figure 3. θ – variation of the normalized stresses for Figure 1(a) $(n = 3, \lambda = 90^{\circ})$.

Table 1. The values of s and the crack I ($n = 3$)

λ	0°	15°	30°	45°	60°	75°	90°	105°	120°
$\mu = 0.00$	-0.25000	-0.249887	0.249035	-0.246551	-0.241165	-0.230951	-0.212612	-0.179875	-0.119537
$\mu = 0.10$	-0.2500	-0.249640	-0.248198	-0.244747	-0.237952	-0.225720	-0.204416	-0.167091	-0.099260
$\mu = 0.20$		-0.249268	-0.247145	-0.242644	-0.234345	-0.219960	-0.195472	-0.153230	-0.073636
$\mu = 0.30$		-0.248749	-0.245866	-0.240205	-0.230260	-0.213520	-0.185536	-0.137872	-0.053164
$\mu = 0.40$			-0.244320	-0.237352	-0.225556	-0.206154	-0.174205	-0.120382	-0.025636
$\mu = 0.50$			-0.242400	-0.233939	-0.219981	-0.197456	-0.160830	-0.099525	>0
$\mu = 0.60$				-0.229691	-0.213079	-0.186683	-0.144227	-0.074020	>0
$\mu = 0.70$				-0.223998	-0.203867	-0.172237	-0.121821	-0.039078	>0
$\mu = 0.80$					-0.189321	-0.149108	-0.085345	>0	>0
$\mu = \mu_{\text{lim}}$	0.187	0.374	0.584	0.773	0.857	0.865	0.866	0.774	0.480
s	-0.250000	-0.245673	0.237134	-0.215824	-0.170827	-0.102627	-0.002249	-0.000395	-0.000132

Table 2. The values of s for crack I $(n = 6)$

λ	0°	15°	30°	45°	60°	75°	90°	105°	120°
$\mu = 0.00$	-0.142857	-0.142817	0.142541	-0.141709	-0.139799	-0.135910	-0.128250	-0.112765	-0.079269
$\mu = 0.10$	-0.142857	-0.142734	-0.142246	-0.141044	-0.138552	-0.133736	-0.124501	-0.106094	-0.068042
$\mu = 0.20$	-0.142857	-0.142604	-0.141861	-0.140244	-0.137108	-0.131264	-0.120256	-0.098552	-0.052821
$\mu = 0.30$	-0.142857	-0.142427	-0.141380	-0.139291	-0.135428	-0.128407	-0.115354	-0.089850	-0.036816
$\mu = 0.40$		-0.142192	-0.140786	-0.138148	-0.133437	-0.125028	-0.109542	-0.079534	-0.018006
$\mu = 0.50$			-0.140004	-0.136745	-0.131004	-0.120890	-0.102396	-0.066853	>0
$\mu = 0.60$			-0.139073	-0.134953	-0.127889	-0.115555	-0.093125	-0.050411	>0
$\mu = 0.70$				-0.132477	-0.123558	-0.108054	-0.079983	-0.027099	>0
$\mu = 0.80$					-0.116333	-0.095288	-0.057282	>0	>0
$\mu = \mu_{\text{lim}}$	0.346	0.495	0.656	0.790	0.857	0.865	0.866	0.774	0.480
s	-0.142857	-0.140992	0.139051	-0.127915	-0.106556	-0.070643	-0.001581	-0.000279	-0.00094

Table 3. The values of s and the crack I $(n = 10)$

λ	0°	15°	30°	45°	60°	75°	90°	105°	120°
$\mu = 0.00$	-0.090909	-0.090893	0.090785	-0.090458	-0.089679	-0.088016	-0.084530	-0.076731	-0.057019
$\mu = 0.10$	-0.090909	-0.090859	-0.090665	-0.090180	-0.089140	-0.087035	-0.082705	-0.073700	-0.048851
$\mu = 0.20$	-0.090909	-0.090806	-0.090505	-0.089838	-0.088503	-0.085888	-0.080569	-0.068751	-0.039267
$\mu = 0.30$	-0.090909	-0.090733	-0.090300	-0.089423	-0.087746	-0.084529	-0.078017	-0.063545	-0.027825
$\mu = 0.40$	-0.090909	-0.090635	-0.090043	-0.088916	-0.086829	-0.082875	-0.074876	-0.057093	-0.013839
$\mu = 0.50$		-0.090504	-0.089718	-0.088283	-0.085683	-0.080785	-0.070853	-0.048785	>0
$\mu = 0.60$			-0.089290	-0.087456	-0.084174	-0.077990	-0.065386	-0.032475	>0
$\mu = 0.70$				-0.086284	-0.082000	-0.073877	-0.057200	-0.020588	>0
$\mu = 0.80$					-0.078184	-0.066414	-0.042037	>0	>0
$\mu = \mu_{\text{lim}}$	0.444	0.566	0.691	0.798	0.856	0.865	0.866	0.774	0.480
s	-0.090909	-0.090121	0.088201	-0.083863	-0.072873	-0.050649	-0.001218	-0.000216	-0.000073

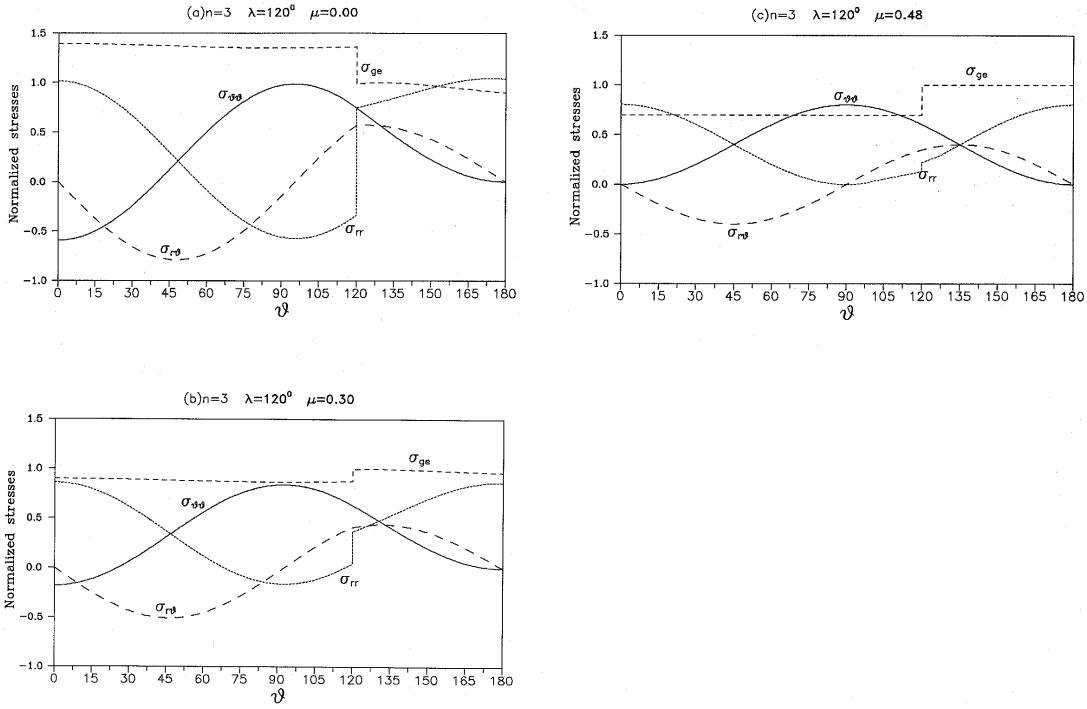

Figure 4. θ – variation of the normalized stresses for Figure 1(a) ($n = 3, \lambda = 120^{\circ}$).

3. Solution for asymptotic fields for cracks I as shown in Figure 1(a)

Combining the nonlinear Equations (15) for plane strain and the boundary conditions (19) and (25), the eigenvalue s and eigenfunction F on the region $\lambda \leqslant \theta \leqslant \pi$ for the pressure-sensitive material 1 can be found using the shooting method. The initial value of $F(\lambda)$ is taken as unity for simplicity. After s is preferred to $-1/(1+n)$ and a value of $F'(\lambda^+)$ is given, $F''(\lambda^+)$ and $F'''(\lambda^+)$ can be obtained from (25), by using the fourth order Runge-Kutta method with automatic step-size control. Equation (15) can be integrated from $\theta = \lambda^+$ to $\theta = \pi$. The results at $\theta = \pi$ generally cannot fully satisfy the boundary conditions. Then, adjust s and the initial value of $F'(\lambda^+)$ step by step and repeat the process until the conditions (19) are satisfied within the limit of error required.

After $F(\lambda^+)$ and $F'(\lambda^+)$ are obtained for the pressure-sensitive material, the coefficients B_1 and B_3 in Equation (17) can be determined by employing the conditions (19) and (21).

For various λ and μ, the eigenvalues s are given in Tables 1, 2 and 3 respectively for $n = 3$, 6 and 10. The θ-variations of the stresses $\widetilde{\sigma}_{ij}$ and $\widetilde{\sigma}_{ge}$ are presented in Figures 2–7 for $n = 3$ and 10. The solutions for $n = 3$ and $n = 10$ represent the crack-tip field for typical high-hardening and low-hardening materials, respectively. All the stresses are normalized by setting the maximum value of generalized effective stress $\widetilde{\sigma}_{ge}$ equal to unity.

When $\lambda = 90^{\circ}$ and $\mu = 0.0$, it becomes a problem for the crack perpendicular to the interface of the classical elastic-plastic material and linear material which was considered by Wang (1990). Our results as shown in Figures 3 and 6 coincide with those given in Wang (1990).

Table 4. The critical angle θ_0 for crack I

	$n = 3$	$n = 6$	$n = 10$
$\mu = 0.00$	100.6°	96.3°	94.0°
$\mu = 0.10$	100.0°	96.0°	93.9°
$\mu = 0.20$	99.3°	95.7°	93.8°
$\mu = 0.30$	98.6°	95.4°	93.6°
$\mu = 0.40$	97.9°	95.0°	93.4°
$\mu = 0.50$	97.0°	94.6°	93.2°
$\mu = 0.60$	96.1°	94.1°	92.9°
$\mu = 0.70$	94.9°	93.4°	92.5°
$\mu = 0.80$	93.2°	92.3°	91.7°

In the case of $\lambda < 90°$, a μ_{lim} exists for each n. When $\mu = \mu_{\text{lim}}$, the numerical result of generalized effective stress σ_{ge} at $\theta = \lambda$ for the pressure-sensitive dilatant material approaches 0. When $\mu \geqslant \mu_{\text{lim}}$, we cannot find any solution based on the HRR-type formulation. This is similar to that given in Li and Pan (1990).

In the case of $\lambda > 90°$, also exists a μ_{lim}. The eigenvalue s is greater than zero when $\mu > \mu_{\text{lim}}$.

Figures 8 and 9 show the displacements $\widetilde{u}_{ij}$ near the crack tip for $n = 6$ and various λ and μ. It is clearly visible that the conditions (24) are exactly met and the crack faces obviously open.

3.1. The effect of parameter λ on asymptotic fields

From Tables 1–3, it can be seen that the eigenvalue s increases as λ increases for the same μ. When λ is equal to a certain value (for example, $\lambda = 135°$, for $n = 3$, 6 or 10) the eigenvalue s is greater than zero for all μ. It means that the singularity disappears near the crack tip.

From Figures 2–7 it is interesting to find that the parameter λ has a strong effect on the jump value in the radial stress across the material interface, $(\widetilde{\sigma}_{rr}|_{\lambda^+} - \widetilde{\sigma}_{rr}|_{\lambda^-})$. For $\mu = 0.0$, when λ is small, the jump value $(\widetilde{\sigma}_{rr}|_{\lambda^+} - \widetilde{\sigma}_{rr}|_{\lambda^-})$ is greater than zero, and as λ arrives at a certain value it becomes negative, then positive again when λ continues to increase.

Generally, there exists a critical angle θ_0 for each n and μ. When $\lambda < \theta_0, \sigma_{\theta\theta}$ has peak value in the symmetric face and $\widetilde{\sigma}_{r\theta}$ is always positive in the whole field. However, when $\lambda \geqslant \theta_0, \widetilde{\sigma}_{r\theta}$ has peak value near 90° and a minimum value at the symmetric face, and $\widetilde{\sigma}_{r\theta}$ is negative in the region between 0° and 90°. Table 4 lists the θ_0 for various n and μ.

3.2. The effect of pressure sensitivity parameter μ on the near-tip field

From Tables 1–3 it can be seen that the eigenvalue s increase as μ increases. When $\lambda < 90°$ the eigenvalue s is always negative for all the μ. When $\lambda > 90°$ the eigenvalue may be positive for a certain value of μ.

From Figures 2–7 it can be seen that the pressure sensitivity parameter μ has little effect on the stresses $\widetilde{\sigma}_{ij}$ except for the small λ. When λ is small, the $(\widetilde{\sigma}_{rr}|_{\lambda^+} - \widetilde{\sigma}_{rr}|_{\lambda^-})$ changes from positive to negative as μ increases.

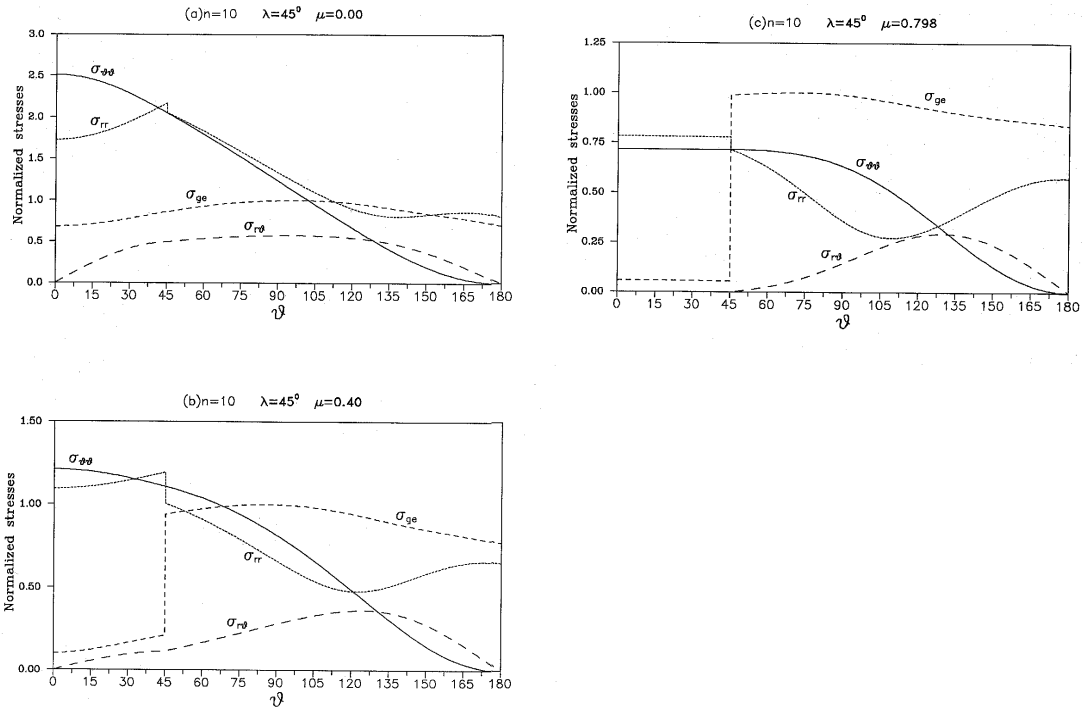

Figure 5. θ – variation of the normalized stresses for Figure 1(a) $(n = 10, \lambda = 45^{\circ})$.

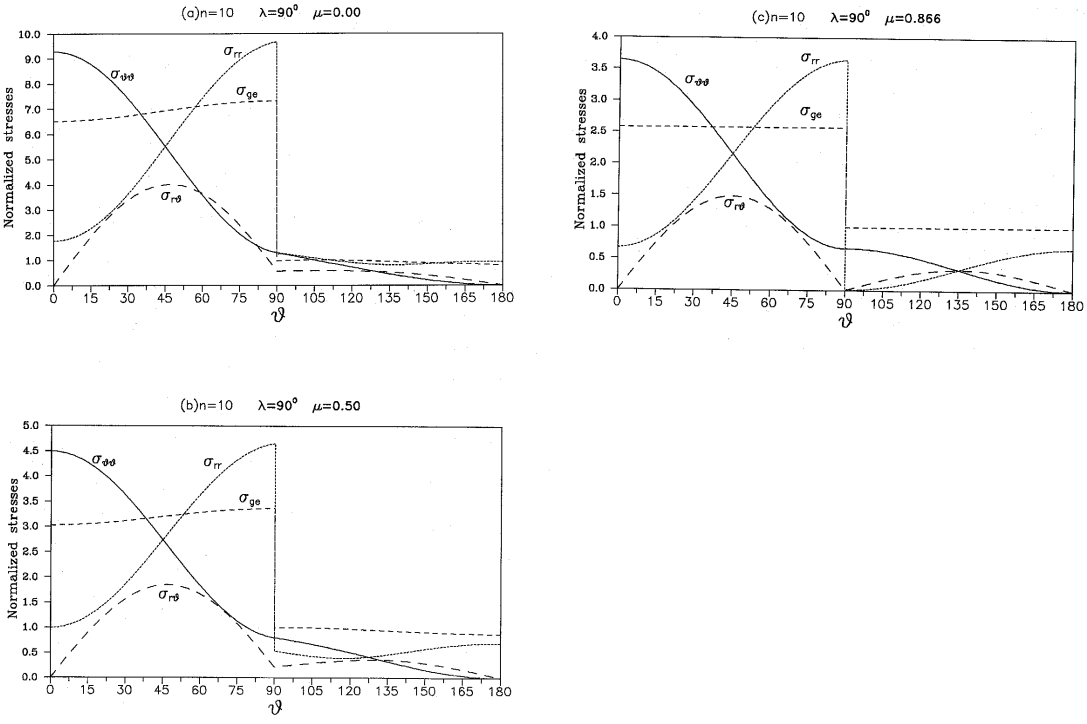

Figure 6. θ – variation of the normalized stresses for Figure 1(a) $(n = 10, \lambda = 90^{\circ})$.

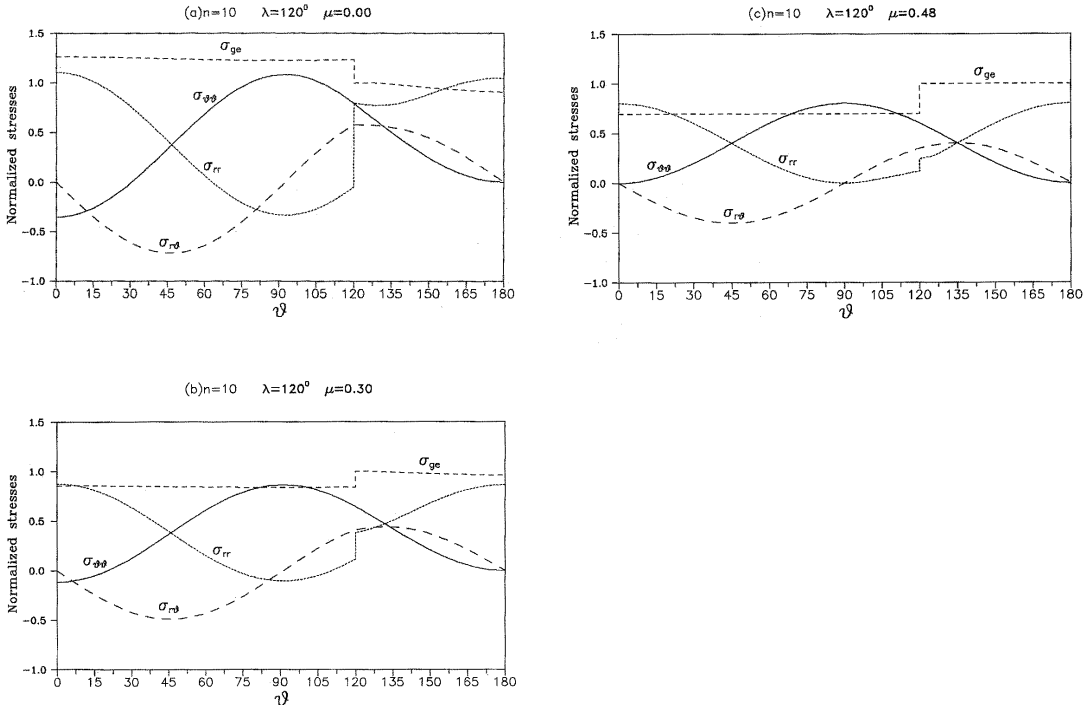

Figure 7. θ – variation of the normalized stresses for Figure 1(a) $(n = 10, \lambda = 120^\circ)$.

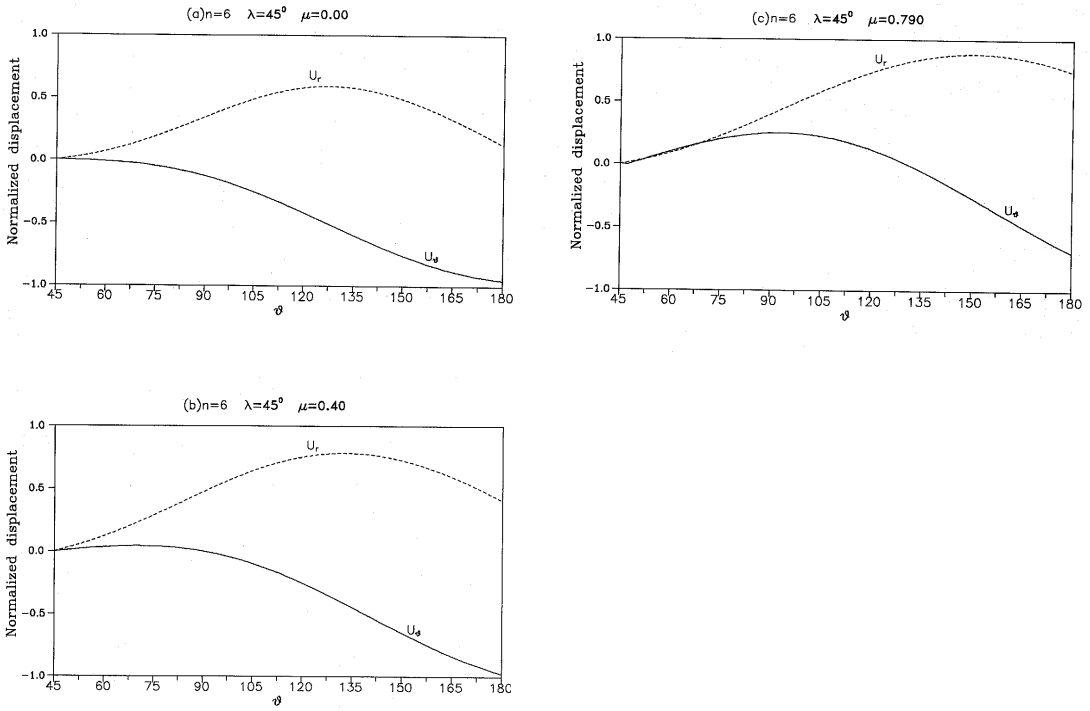

Figure 8. Angular distribution of displacements for Figure 1(a) $(n = 6, \lambda = 45^\circ)$.

Table 5. The values of s for crack II ($n = 3$)

λ	0°	15°	30°	45°
$\mu = 0.00$	-0.250000	-0.203528	-0.132769	-0.036687
$\mu = 0.10$	-0.250000	-0.206072	-0.142312	-0.050305
$\mu = 0.20$	-0.250000	-0.208969	-0.148532	-0.061045
$\mu = 0.30$		-0.212513	-0.155459	-0.071256
$\mu = 0.40$		-0.217145	-0.163941	-0.082554
$\mu = 0.50$			-0.175349	-0.097148
$\mu = 0.60$			-0.192326	-0.113293
$\mu = 0.70$				-0.158163
$\mu = \mu_{\text{lim}}$	0.254	0.469	0.631	0.740
s	-0.250000	-0.221365	-0.199472	-0.182684

Table 6. The values of s for crack II ($n = 6$)

λ	0°	15°	30°	45°
$\mu = 0.00$	-0.142857	-0.120392	-0.084354	-0.021464
$\mu = 0.10$	-0.142857	-0.120939	-0.087172	-0.029927
$\mu = 0.20$	-0.142857	-0.121695	-0.089176	-0.036047
$\mu = 0.30$	-0.142857	-0.122296	-0.092136	-0.041768
$\mu = 0.40$		-0.125013	-0.096090	-0.048209
$\mu = 0.50$		-0.128509	-0.101833	-0.056700
$\mu = 0.60$			-0.111058	-0.069559
$\mu = 0.70$				-0.091771
$\mu = \mu_{\text{lim}}$	0.397	0.547	0.663	0.755
s	-0.142857	-0.131055	-0.120575	-0.112941

3.3. THE EFFECT OF VARYING n

It is clearly visible from Tables 1–3 that the eigenvalue s increases as n increases.

Comparing Figures 2–4 with Figures 5–7 respectively it was found that the stress components are slightly affected by the changing n in the pressure-sensitive dilatant material. The effect of varying s on the stresses in elastic material is larger than that in material 1.

4. Solution for crack II as shown in Figure 1(b)

Figure 1(b) shows another type of crack that lies in medium 1 and its tip touches the interface of media 1 and 2. The external load is also assumed to be symmetric remote tension.

For material 1 the traction-free conditions on the crack faces require

$$\sigma_{\theta\theta}|_{\theta=0} = \sigma_{r\theta}|_{\theta=0} = 0. \tag{26}$$

For material 2 the symmetry condition requires

$$u_\theta|_{\theta=\pi} = \sigma_{r\theta}|_{\theta=\pi} = 0 \tag{27}$$

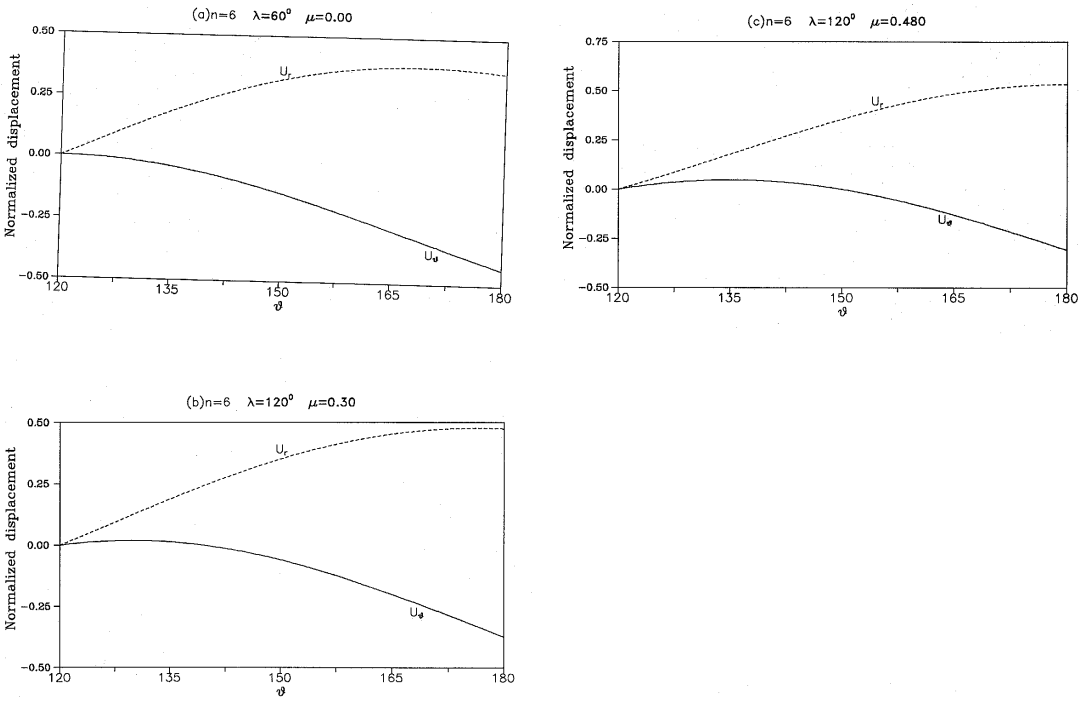

Figure 9. Angular distribution of displacements for Figure 1(a) ($n = 6, \lambda = 120^\circ$).

or

$$F'(\pi) = F'''(\pi) = 0. \tag{28}$$

Using the same method as stated above, we obtain the solution in this case. The eigenvalue s for the various λ and μ are given in Tables 5 and 6 for $n = 3$ and 6, respectively. The numerical results show that the eigenvalue s for $\lambda > 50.5^\circ$ is larger than zero. Therefore, we give the numerical results only for $\lambda = 0^\circ, 15^\circ, 30^\circ$ and 45°. From these tables it can be seen that the eigenvalue s increases as λ increases for the same μ. However, for the same n and λ the eigenvalue s decreases as μ increases. This is different from what we discussed above.

Figures 10 and 11 show the θ-variations of the stresses $\widetilde{\sigma}ij$ with $n = 6$ for $\lambda = 15^\circ, 30^\circ$ and $\mu = 0.0, \mu_{\text{mid}}, \mu_{\text{lim}}$. The μ_{mid} is a middle value between 0.0 and μ_{lim}. The stresses are normalized by setting $(\widetilde{\sigma}_{ge})_{\max}$ in the elastic region equal to unity. It can be seen that the parameter μ has little effect on the stresses $\widetilde{\sigma}_{ij}$ for the pressure-sensitive dilatant materials. However, μ has an effect on the distribution of stresses $\widetilde{\sigma}_{rr}$. $\widetilde{\sigma}_{rr}$ increases as θ increases for the small μ. On the contrary, $\widetilde{\sigma}_{rr}$ decreases as θ increases for the larger θ. For other n and λ we have obtained similar results.

5. Conclusion

1. Based on the pressure-sensitive yielding criterion, we obtained exact asymptotic solutions for the stress-strain field near the crack tip for two types of cracks which satisfy the continuity of tractions and displacements on the interface and traction-free conditions on the crack faces. The present results show that the stress distributions near the crack tip are quite similar to those of the HRR singularity field.

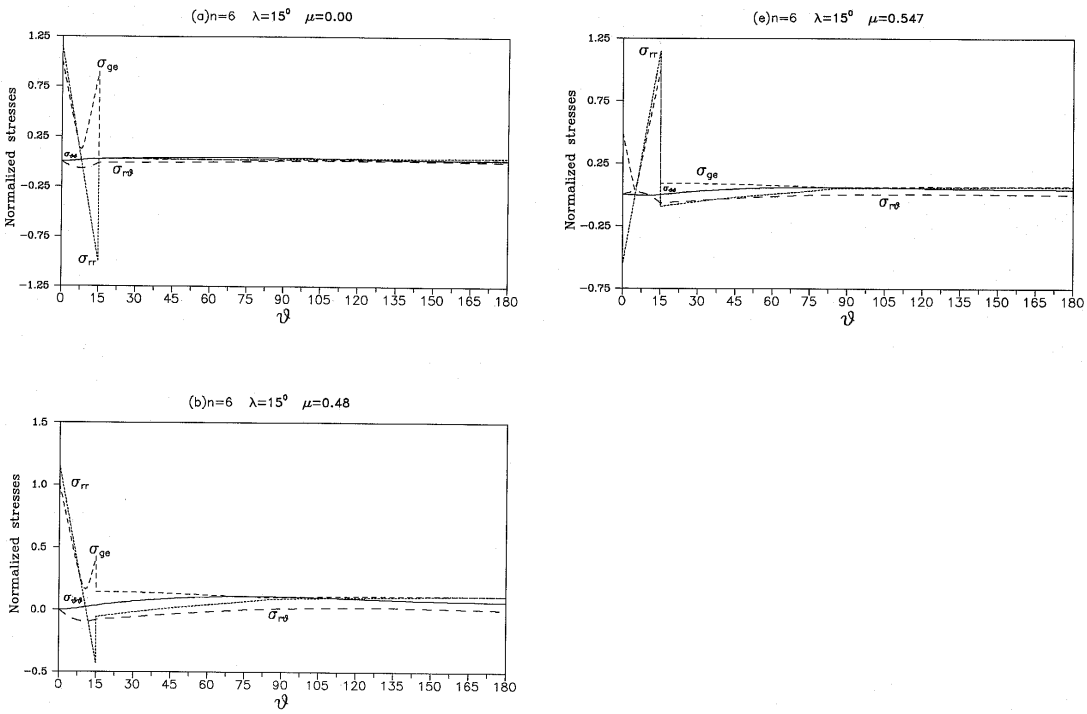

Figure 10. θ – variation of the normalized stresses for Figure 1(b) ($n = 6, \lambda = 15^{\circ}$).

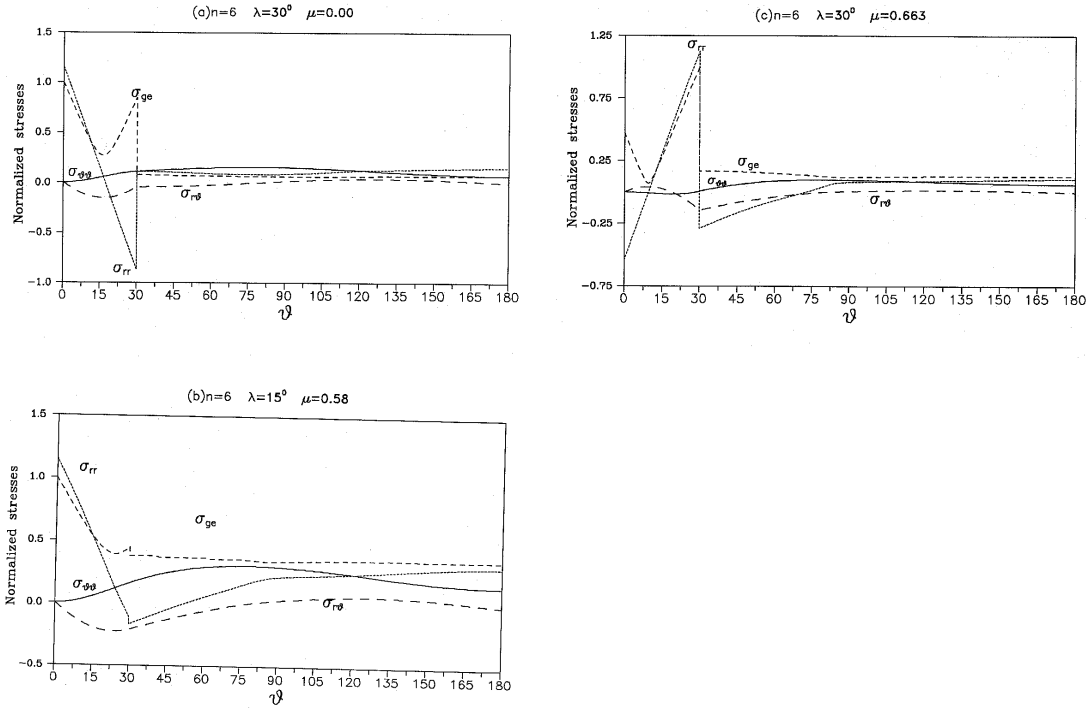

Figure 11. θ – variation of the normalized stresses for Figure 1(b) ($n = 6, \lambda = 30^{\circ}$).

2. For crack I which lies in the pressure-sensitive dilatant material, the eigenvalue s increases as λ increases. The parameter λ has a strong effect on the distribution of the radial stress along the circumferential direction. The eigenvalue s increases too as the material constant μ or n increases.

The stress components in the pressure-sensitive dilatant material are slightly affected by the changing μ or n.

3. For crack II which lies in the elastic material, the eigenvalue s increases as λ increases, but decreases as μ increases. The parameter μ has a slight effect on the stresses in the pressure-sensitive dilatant material. However, it has an effect on the distribution of stress $\widetilde{\sigma}_{rr}$.

Acknowledgments

The work was supported by the National Natural Science Foundation of China, Science Foundation of Chinese Academy of Sciences and Laboratory for Nonlinear Mechanics of Continuous Media, Institute of Mechanics.

References

Carapellucci, L.M. and Yee, A.F. (1986). The biaxial deformation and yield behaviour of bisphenol-a polycarbonate: effect of anisotropy. *Polymer Engineering and Science* **26**, 920–930.

Chen, I.W. and Morel, P.E.R. (1986). Implications of transformation plasticity in ZrO_2-containing ceramics: I shear and dilatation effect. *Journal of America Ceramic Society* **69**, 181–189.

Chevpanov, G.P. (1962). The stress state in a heterogeneous plate with slits. Izv. AN SSSR, OTH *Mekhan i Mashin* **1**, 131–137.

Cook, T.S. and Erdogan, F. (1972). Stresses in bounded materials with a crack perpendicular to the interface. *International Journal of Engineering Sciences* **10**, 677–689.

Drucker, D.C. and Prager, W. (1952). Soil mechanics and plastic analysis or limit design. *Quarterly Journal of Applied Mathematics* **10**, 157–165.

Erdogan, F. (1965). Stress distribution in bounded dissimilar materials with cracks, *Journal of Applied Mechanics* **32**, 403–410.

Hutchinson, J.W., Mear, M. and Rice, J.R. (1987). Crack paralleling an interface between dissimilar material. *Journal of Applied Mechanics* **54**, 828–832.

Li, F.Z. and Pan, J. (1990). Plane strain crack-tip fields for pressure-sensitive dilatant materials. *Journal of Applied Mechanics* **57**, 40–47.

Malyshev, B.M. and Salganik, R.L. (1965). The strength of adhesive joints using the theory of cracks. *International Journal of Fracture Mechanics* **1**, 114–128.

Parks, D.M. and Zywicz, E. (1989). Elastic/perfectly-plastic small-scale yielding at bimaterial interfaces. *Advances in Fracture Research*. edited by Salama et al., Vol. 4, 3081–3088.

Rice, J.R. (1988). Elastic fracture mechanics concepts for interfacial cracks. *Journal of Applied Mechanics* **55**, 98–103.

Rice, J.R. and Sih, G.C. (1965). Plane problems of cracks in dissimilar media. *Journal of Applied Mechanics* **32**, 400–402.

Shih, C.F. and Asaro, R.J. (1988). Elastic-plastic analysis of cracks on bimaterial interface: part I – small scale yielding. *Journal of Applied Mechanics* **55**, 299–316.

Shih, C.F. and Asaro, R.J. (1989). Elastic-plastic analysis of cracks on bimaterial interface: part II – structure of small scale yielding. *Journal of Applied Mechanics* **56**, 763–779.

Shih, C.F. and Asero, R.J. (1990). Elastic-plastic and asymptotic fields of interface cracks. *International Journal of Fracture* **42**, 101–116.

Sih, G.C. and Rice, J.R. (1963). The bending of plates in dissimilar materials with cracks. *Journal of Applied Mechanics* **30**, 232–236.

Spitzig, W.A. and Richmond, O. (1979). Effect of hydrostatic pressure on the deformation behaviour of polythene and polycarbonate in tension and compression. *Polymer Engineering and Science* **19**, 1129–1139.

Sue, H.J. and Yee, A.F. (1989). Toughening mechanisms in a multi-phase alloy of nylon 6,6/polyphenylene oxide, *Journal of Materials Science* **24**, 1447–1457.

Wang, T.C. (1990). Elastic-plastic asymptotic fields for cracks on bimaterial interfaces. *Engineering Fracture Mechanics* **37**, 527–538.

Williams, M.L. (1959). The stress around a fault or crack in dissimilar media. *Bulletin of Seismological Society of America* **49**, 199–204.
Yuan, H. (1994/1995). Elastoplastic crack analysis for pressure-sensitive dilatant material – part II: interface cracks. *International Journal of Fracture* **69**, 167–187.
Zywicz, E. and Park, D.M. (1989). Elastic yield zone around an interfacial crack tip. *Journal of Applied Mechanics* **56** 577–584.